International Journal of Remote Sensing
July 2013, Volume 34, Issue 14, pages 5243-5261
http://dx.doi.org/10.1080/01431161.2013.787502

Improvement in air–sea flux estimates derived from satellite observations

Abderrahim Bentamy[a, *], Semyon A. Grodsky[b], Kristina Katsaros[c], Alberto M. Mestas-Nuñez[d], Bruno Blanke[e] & Fabien Desbiolles[a, e]

[a] Laboratoire d'Océanographie Spatiale (LOS), Institut Français pour la Recheche et l'Exploitation de la Mer (IFREMER), France
[b] Department of Atmospheric and Oceanic Science, University of Maryland, College Park, MD, USA
[c] Rosenstiel School of Marine and Atmospheric Science, University of Miami, Miami, FL, USA
[d] Department of Physical and Environmental Sciences, Texas A&M University-Corpus Christi, Corpus Christi, TX, USA
[e] Laboratoire de la Physique des Océans (LPO), UMR 6523 CNRS-Ifremer-IRD-UBO, France

*: Corresponding author : Abderrahim Bentamy, email address : abderrahim.bentamy@ifremer.fr

Abstract:

A new method is developed to estimate daily turbulent air–sea fluxes over the global ocean on a 0.25° grid. The required surface wind speed (w_{10}) and specific air humidity (q_{10}) at 10 m height are both estimated from remotely sensed measurements. w_{10} is obtained from the SeaWinds scatterometer on board the QuikSCAT satellite. A new empirical model relating brightness temperatures (T_b) from the Special Sensor Microwave Imager (SSM/I) and q_{10} is developed. It is an extension of the author's previous q_{10} model. In addition to T_b, the empirical model includes sea surface temperature (SST) and air–sea temperature difference data. The calibration of the new empirical q_{10} model utilizes q_{10} from the latest version of the National Oceanography Centre air–sea interaction gridded data set (NOCS2.0). Compared with mooring data, the new satellite q_{10} exhibits better statistical results than previous estimates. For instance, the bias, the root mean square (RMS), and the correlation coefficient values estimated from comparisons between satellite and moorings in the northeast Atlantic and the Mediterranean Sea are –0.04 g kg^{-1}, 0.87 g kg^{-1}, and 0.95, respectively. The new satellite q_{10} is used in combination with the newly reprocessed QuikSCAT V3, the latest version of SST analyses provided by the National Climatic Data Center (NCDC), and 10 m air temperature estimated from the European Centre for Medium-Range Weather Forecasts (ECMWF) reanalyses (ERA-Interim), to determine three daily gridded turbulent quantities at 0.25° spatial resolution: surface wind stress, latent heat flux (LHF), and sensible heat flux (SHF). Validation of the resulting fields is performed through a comprehensive comparison with daily, *in situ* values of LHF and SHF from buoys. In the northeast Atlantic basin, the satellite-derived daily LHF has bias, RMS, and correlation of 5 W m^{-2}, 27 W m^{-2}, and 0.89, respectively. For SHF, the statistical parameters are –2 W m^{-2}, 10 W m^{-2}, and 0.94, respectively. At global scale, the new satellite LHF and SHF are compared to NOCS2.0 daily estimates. Both daily fluxes exhibit similar spatial and seasonal variability. The main departures are found at latitudes south of 40° S, where satellite latent and sensible heat fluxes are generally larger.

1. Introduction

Accurate turbulent air–sea fluxes (i.e. momentum, latent heat, and sensible heat) are of great interest in regard to a wide variety of air–sea interaction issues. The main sources of such fluxes over the global ocean are numerical weather prediction (NWP) models, voluntary observing ships (VOSs), and remotely sensed data.

For over a decade, several scientific groups have been developing direct and inverse methods, algorithms, and procedures to calculate long time series of surface winds, wind stress, specific air humidity, and latent and sensible heat fluxes; representative data sets include the Japanese Ocean Flux data sets with the Use of Remote sensing Observations (J-OFURO) (Kubota et al. 2002), the Goddard Satellite-based Surface Turbulent Fluxes (GSSTF) (Chou et al. 2003), the Objectively Analysed Air–Sea Fluxes (OAFLUX) (Yu, Weller, and Sun 2004), the Institut Français pour la Recherche et l'Exploitation de la Mer (IFREMER) (Bentamy et al. 2003, 2008), and the Hamburg Ocean Atmosphere Parameters and Fluxes from Satellite Data (HOAPS) (Anderson et al. 2010). These satellite fluxes are widely used by the scientific community for various purposes such as forcing ocean circulation models (e.g. Ayina et al. 2006), studying the spatial and temporal variability associated with the El Niño Southern Oscillation (ENSO) (e.g. Mestas-Nuñez, Bentamy, and Kristina 2006), or employing an enhanced spatial and temporal sampling provided by remote techniques to evaluate intra-seasonal variability (e.g. Grodsky et al. 2009). Even though the results of these investigations have increased our understanding of air–sea interactions, further improvements of satellite-based fluxes are still required.

A number of studies assessing the quality of turbulent fluxes have been published in recent years. By comparing latent heat fluxes (LHFs) from buoys and satellites, Bourras (2006) has found that the overall accuracy is of the order of 20–30%, whereas the required error for a quantitative use over the global oceans should be lower than 10%. He has concluded that the main LHF error sources are related to the accuracy of the specific air humidity (q) and surface wind speed (w). Tomita and Kubota (2006) have investigated the accuracy of satellite-based LHF through comparisons with buoy and NWP estimates. In the tropics, the main source of buoy and satellite LHF discrepancy is attributed to the accuracy of satellite q, whereas around Japan the LHF discrepancy is associated with the accuracy of both w and q. They both have concluded that the improvement in satellite LHF estimation requires improvements in remotely sensed w and q

at global and regional scales. Santorelli *et al* (2011) have conducted detailed accuracy investigations of IFREMER and OAFLUX latent and sensible heat fluxes as well as of basic bulk variables (10 m wind speed, W_{10}; 10m specific air humidity, Qa_{10}; 10 m air temperature, Ta_{10}; and SST) using standard moored buoy and dedicated-experiment scientific data. Their conclusions generally agree with the studies mentioned earlier. In particular, they emphasized that the improvement of satellite fluxes should include the improvement of the interpolation method used to calculate gridded fields over the global ocean to better reflect conditions during synoptic-scale storms and fronts.

Following the suggested recommendations improving the fluxes, the present study aims at enhancing the following three aspects: the determination of Qa_{10} retrievals over global oceans, the accuracy of bulk variables as well as of the turbulent fluxes themselves, and the spatial and temporal resolutions of the flux fields. This study takes advantage of the availability of the new air-sea interaction datasets estimated from the updated International Comprehensive Ocean-Atmosphere Data Set (ICOADS) (Berry *et al.*, 2011), and of the new QuikSCAT wind retrievals (Fore *et al.*, 2011) .

A description of the various datasets used is given in section 2 and the method retrieving Qa_{10} from satellite radiometer measurements is presented in section 3. The validation of the resulting flux field analyses is provided and discussed in sections 4 and 5. Finally, section 6 presents the summary, conclusion, and perspective study.

2. Data

The main basic bulk variables required for turbulent flux estimations are surface wind speed (W), specific air humidity (Qa), specific surface humidity (Qs), air temperature (Ta), and sea surface temperature (SST) . Moored buoys, ships, and NWP models provide valuable estimates of these variables with various spatial and temporal resolutions. They are used in this study for the calibration and/or validation of satellite retrievals at local, regional, and global scales.

2.1 Scatterometer data

To ensure homogeneity of W and its variability, this study employs only wind retrievals from SeaWinds scatterometer onboard QuikSCAT. The QuikSCAT scatterometer principle is described in many scientific papers. Readers may find complete description in (JPL, 2006) including instrument physics, retrieval and ambiguity removal methods, rain detection and flagging techniques, and quality control procedures. Briefly, QuikSCAT is a rotating antenna with two differently polarized emitters: the H-pol with incidence angle of 46.25° and V-pol with incidence angle of 54°. The inner beam has a swath width of about 1400km, while the outer beam swath is 1800km width. QuikSCAT

scatterometer is a Ku band radar. Therefore, rain has a substantial influence on its measurements. Previous studies showed that the rain impact may attenuate the scatterometer signal, resulting in wind speed underestimation, or change the surface shape due to raindrop impacts leading to W overestimation in the retrieved winds. QuikSCAT wind products involve several rain flag determined from the scatterometer observations and from the collocated radiometer rain rate onboard other satellites.

This study uses a new QuikSCAT wind retrievals indicated as QuikSCAT *V3* (ftp://podaac.jpl.nasa.gov/OceanWinds/quikscat/preview/L2B12/v3/). They are made available by Jet Propulsion Laboratory (JPL)/ Physical Oceanography Distributed Active Archive Center (PODAAC) scientific team (Fore *et al*, 2011). QuikSCAT *V3* products are calculated based on the use of a geophysical model function ensuring the consistency with winds retrieved from microwave radiometers such as Special Sensor Microwave Imager (SSM/I) and WindSat (Ricciardulli *et al*, 2011). Wind retrievals are provided over QuikSCAT swath at Wind Vector Cell (WVC) of 12.5km spatial resolution. This new scatterometer product is assumed improving wind speed performance in rain and at high wind speed conditions.

The accuracy of the QuikSCAT *V3* data is determined through various comparisons with buoy wind measurements, QuikSCAT *V2* retrievals, and with remotely sensed winds derived from the ASCAT scatterometer onboard Metop-A satellite. The main findings (not shown) are that the comparison results meet those obtained previously (Bentamy *et al*, 2012). QuikSCAT *V3* and QuikSCAT *V2* exhibit similar comparison results versus buoys. ASCAT and QuikSCAT *V3* statistics are of the same order as ASCAT and QuikSCAT *V2*. Discrepancies characterizing ASCAT and QuikSCAT *V2* comparisons are found for ASCAT and QuikSCAT V3. For instance, the most significant discrepancies are found at tropical and high latitudes. QuikSCAT *V3* are corrected and improved when compared with (Bentamy *et al*, 2012) results.

2.2 Radiometer data

The special sensor microwave imager (SSM/I) measurements used in this study are the same as in (Bentamy *et al*, 2003 and 2008). The SSM/I radiometers onboard the Defense Meteorological Satellite Program (DMSP) F11, F13, F14, and F15 satellites provide measurements of the surface brightness temperatures (Tb) at frequencies 19.35, 22.235, 37, and 85 GHz (hereafter referred to as 19, 22, 37, and 85 GHz), respectively. Horizontal and vertical polarization measurements are taken at 19, 37, and 85 GHz. Only vertical polarization is available at 22 GHz. Due to the choice of the channels operating at frequencies outside strong absorption lines (for water vapor 50-70 GHz), the detected radiation is a mixture of radiation emitted by clouds, water vapor in the air and the sea surface, as well as radiation emitted by the atmosphere and reflected at the sea surface. Brightness

temperature measurements as well as the associate geophysical parameters are provided by Global Hydrology Resource Center (GHRC) (http://ghrc.msfc.nasa.gov/)

2.3 Buoys

Data from a number of moored buoys located in different basins are used for the ground truth validation. These include 8 Atlantic moorings off the French and England coasts maintained by UK Met-Office and/or Météo-France (MFUK), 96 moorings off the Atlantic and Pacific U.S coasts maintained by the National Data Buoy Center (NDBC), 66 moorings of the TAO/TRITON array in the equatorial Pacific, and 13 moorings of the PIRATA network in the equatorial Atlantic. TAO/TRITON and PIRATA will be hereafter referred as tropical buoys. Meteorological buoy data are hourly average. Measurement height varies between 3m and 10m depending on mooring configuration Buoy wind, specific air humidity, air temperature are converted to the standard height of 10m using the COARE3.0 algorithm of Fairall *et al*. (2003). The latter is also used to estimate buoy turbulent fluxes.

2.4 NOCS data

A new daily mean air-sea interaction gridded dataset (Berry *et al*, 2011) is provided by the National Oceanography Centre Southampton and referred as NOCS Flux Dataset v2.0 (NOCS2.0). They are available over global ocean with a spatial resolution of 1° in longitude and latitude. Daily parameters such as W_{10}, Qa_{10}, Ta_{10}, SST, Latent heat (LHF) and sensible (SHF) are provided with uncertainty estimates. The accuracy of NOCS2.0 gridded parameters was investigated trough various comparisons including buoy, satellite, and numerical model data. For instance the comparison with buoys deployed and maintained by the Woods Hole Oceanographic Institution (WHOI) Upper Ocean Processes Group (UOP) indicates that the mean difference (NOCS2.0 – WHOI UOP) of W_{10} and Qa_{10} are about 0.30m/s ans 0.40g/kg, respectively (Table II of Berry *et al*, 2011)

2.5 Era Interim

Era-Interim (Simmons *et al*., 2006) refers to the re-analyses of atmospheric parameters produced by the European Center for Medium Weather Forecasts (ECMWF). It uses 4D-variational analysis on a spectral grid. This re-analysis covers the period from 1989 to the present day. The ERA-Interim data used in this study was obtained from the ECMWF data server on a fixed grid of 0.75°. The main parameters used in this study are specific air humidity and air temperature at 2m, available at synoptic times (00h:00, 06h:00, 12h:00, 18h:00 UTC), converted to Qa_{10} and to Ta_{10} ,

respectively, utilizing the COARE3.0 model (Fairall *et al*, 2003). The quality of Qa_{10} and of Ta_{10} is checked through comparisons with MFUK, TAO, and PIRATA buoy estimates. The main finding of interest for this study, is that Era Interim Ta_{10} are underestimated for buoy Ta_{10} exceeding 20°C. A bias correction is determined from linear regression between Era Interim and buoy Ta_{10} estimates.

2.6 Collocation

For Qa calibration purpose, SSM/I, NOCS2.0, Era Interim and SST are collocated in space and time. SST data are version 2 of IO daily analyses (Reynolds *et al*, 2007) with a spatial resolution of 0.25° in longitude and latitude. Common collocation procedure is utilized. Era interim Qa_{10} and Ta_{10} occurring within 50km and 3 hours from SSM/I cell location and time, respectively, are bi-linearly interpolated at SSM/I cell. SSM/I brightness temperatures and NOCS2.0 Qa_{10} occurring same day are matched such as the spatial difference is less than 100km. Same collocation approach is used for SSM/I Tb and daily SST, except that the spatial difference criteria is 25km.

3. Specific Air Humidity Improvement

3.1 Retrieving specific air humidity from satellite measurements

Based on the collocated SSM/I and ICOADS data, several authors assessed the relationship between satellite brightness temperatures (Tb) and in-situ specific air temperature (Qa) (e.g. Kubota *et al*, 2008; Jackson *et al*, 2009). The former is mainly related to the quite linear relationship between specific air humidity and the column integrated water vapor content (WV) obtained from satellite microwave radiometers (Schultz *et al*, 1993). SSM/I Tb measurements are sensitive to WV especially in 19v, 19h, 22v, and 37v channels. In (Bentamy *et al*, 2003) the development of a SSM/I-based method for the retrieval of Qa from brightness temperatures is based on a model determined from the collocated SSM/I Tb and COADS Qa over a limited oceanic areas of the North Atlantic and of the eastern equatorial Pacific oceans, and during a limited period (1996 – 1998). This model was successfully used by several groups for Qa estimation from SSM/I or from AMSRE measurements as well as to assess a new development of Qa models (e.g. Anderson *et al*, 2010; Kubota *et al*, 2008; Jackson *et al*, 2009). However, Grodsky *et al* (2009), and Santorelli *et al* (2011) underlined the need for improvement of the remotely sensed specific air humidity. To achieve such enhancement, the new updated and enhanced NOCS2.0 data are used as references for a new Qa_{10} modeling. For instance Figure 1 shows the difference between NOCS2.0 and the previous version of satellite Qa_{10} of Bentamy *et al*. (2003) as a function of satellite-derived Qa_{10} and for five NOCS2.0 SST ranges. The findings (Figure 1) suggest including SST as a variable in a satellite

Qa_{10} model. Furthermore, the investigation of NOCS2.0 and satellite Qa_{10} differences indicates a stratification dependency. The latter would be an indication of the modification of the relationship between WV and Qa as a function of stratification variability. Therefore, the new Qa model includes terms related to SST and to the difference between 10m air and sea surface temperatures (ΔT).

$$Qa_{10} = f_1(TB_{19V}) + f_2(TB_{19H}) + f_3(TB_{22V}) + f_4(TB_{37V}) + g(SST) + h(\Delta T) \quad (1)$$

The functions f_1, f_2, f_3, f_4, , g , and h are determined through a maximum likelihood procedure based on the use of collocated data: SSM/I F11 Tb, NOCS2.0 Qa_{10}, SST, and Era Interim Ta_{10}. Only matchups occurring during January, April, August, and September 2005 are used. Due to the strong correlation between WV and brightness temperatures and between specific air humidity and sea surface temperature, Qa_{10} (eq. 1) is mainly weighted by functions f_1, f_2, f_3, f_4, , g . On overall, the term $h(\Delta T)$ has a small impact. However, it maintains the bias between NOCS2.0 and satellite Qa close to zero with respect to air-sea temperature difference.

Insert Figure1

3.2 Daily analysis

One of the main goals of this study is to estimate daily 10m specific air humidity from remotely sensed data with same spatial resolution as the gridded daily wind fields (see the following section). All available and valid brightness temperature measurements from F11, F13, F14, and F15 satellites during 2005 – 2007 period are used. For each day and for each individual SSM/I swath cell, valid brightness temperatures (instantaneous), and the spatially closest daily averaged SST and 6-hourly 10m air-temperature are selected. Specific air humidity is estimated based on (eq. 1). Due to time differences and accuracy characteristics (Meisnner *et al*, 2001) of brightness temperatures derived from various instruments may contribute to a non consistency between Qa derived from (1) and actual values expected to be used for daily gridded specific air humidity calculation. To reduce the non-consistency impact, auxiliary information providing a mean description of Qa during a given day is also used. It is derived from 6-hourly Era Interim Qa estimates. The following linear relationship between retrievals (Qa_{10}) and auxiliary data is assumed:

$$E(Qa_{10}(x,y,t)) = \alpha_0 + \beta_1 Qamod(x,y,t) \quad (2)$$

Where x, y, and t, state for spatial and temporal coordinates. α_0 and β_1 are coefficients to be

estimated. Operator *E* states for mathematical mean (conventional first moment). Qamod indicates Era Interim Qa_{10} collocated in space and time with each individual satellite retrieval. (2) is known as external drift constraint (Wackernagel, 1998).

The objective method aiming to calculate gridded daily specific air humidity from retrievals is quite similar to the method used for daily ASCAT wind field analyses (Bentamy *et al*, 2011). Briefly, daily satellite Qa is estimated based on the following assumption:

$$Qasat = \frac{1}{(t_b - t_a)} \int_{ta}^{tb} \left(\sum_{j=1}^{N} \lambda_j (Qa_{10}(x_j, y_j, t)\right) dt + \varepsilon \qquad (3)$$

With unbiased constraint $\sum_{j=1}^{j=N} \lambda_j = 1$ and external drift constraint (2)

$Qa_{10}(x_j,y_j,t)$ indicates the jth Qa_{10} retrieval available over a given satellite swath cell with geographical coordinates (x_j, y_j) and at time t. ta and tb indicate the time interval falling within 00h:00mn:00sec and 23h:59mn:59sec when retrievals are available. N is the retrieval number selected for daily analysis calculation.

$\boldsymbol{\lambda}$ is the weighting vector to be estimated. It is the solution of the following linear system:

$$\begin{cases} \sum_{j=1}^{j=N} \lambda_j C_{ij} - \mu_1 - \mu_2 Qa\,\mathrm{mod}\, i = C_{i0} \quad \text{for } i = 1, N \\ \sum_{j=1}^{j=N} \lambda_j = 1 \\ \sum_{j=1}^{j=N} \lambda_j Qa\,\mathrm{mod}_j = Qa\,\mathrm{mod}_0 \end{cases}$$

C_{ij} stands for covariance matrix between Qa observations, while μ_1 and μ_2 are the Lagrangian terms used to take into account the unbiased and external drift constraints. Index 0 indicates grid point where daily analysis is performed.

The objective method requires parameterization of the spatial and temporal covariance structure of specific air humidity. It is determined from retrievals occurring during January, April, July, and October 2005 over the global ocean between 55°S and 55°N.

3.3 Satellite daily Qa_{10} Accuracy

The quality of the resulting satellite daily 10m Qa estimates (Qasat) is mainly investigated through comprehensive comparisons with daily averaged 10m specific air humidity (Qabuoy) from buoys during the 2005 – 2007 period when the new Qasat and the old Qasat_old are both available.

Daily buoy estimates are calculated as arithmetic mean of all valid hourly data. For each day of the period, all daily buoy and satellite data separated by less than 25 km are selected. Consequently, 2910 collocations from MFUK, and 16999 from tropical networks, with specific air humidity ranging from 2g/kg to 25 g/kg met all the collocation quality control criteria. The buoy-satellite comparisons are complimented by comparisons with daily ship data from NOCS2.0 for the two regions: low humidity region in the midlatitude North Atlantic and in the Mediterranean sea 20°W-10°E, 35°N – 60°N, and more humid region in the tropical Atlantic 70°W-10°E, 15°S-15°N. These regions are selected based on the ground truth mooring locations. The northern region hosts the MFUK moorings while the tropical region hosts the PIRATA mooring array. In addition, the quality of daily satellite Qa analysis is investigated on the global scales through comparisons with daily estimates from NOCS2.0 and Era Interim. Only the 2007 NOCS2.0 Qa are used for the global comparisons because these data were excluded from the calibration of Qa model (eq. 1).

Even though buoy as well as ship Qa data are used as ground truth references, both sources may have uncertainties mainly related to hygrometer type, measurement height, and to solar radiation contamination (Kent *et al*, 2007). The assessment of quality of the reference data is beyond the topic of this paper.

To limit possible impacts of sampling errors of in-situ data, comparisons are limited to Qa with relative random error less than 10%. Most of cases (>95%) when this error exceeds 10% occur in dry conditions Qa<4g/kg happening at MFUK buoys. The statistics established for these specific cases yields an overestimation of satellite Qa_{10}.

Figure 2a and 2b illustrate validation results obtained for MFUK and tropical moorings, respectively. The statistics characterizing buoy and satellite comparisons are estimated. Table 1 provides the biases and standard deviations (Std) of buoy and satellite differences (in this order), and correlation coefficients (Cor). The statistics associated with the performance of daily Qa from (Bentamy *et al*, 2003), indicated as Qasat_old, are also provided. The updated daily satellite Qasat gives a good representation of daily in-situ Qa estimates. Correlation coefficients between tropical and satellite, and between MFUK and satellite daily Qa are of 0.85 and 0.95, respectively. At MFUK buoy locations, correlation coefficient varies between 0.92 and 0.95 leading to no significant location dependence. Even though at tropical locations, correlation coefficients are quite high, better results are found at buoys moored off the equatorial area where polar-orbiting satellite sampling is better than at low latitudes. NOCS2.0 and satellite Qa comparisons (Table 1) indicate similar correlation results.

Insert Figure2

Biases for the new Qa product are low (Table 1) and are not statistically significant. Bias increases for low and high mooring Qa (Figure 2a and b) indicating slight overestimation and underestimation, respectively, which is also evident from the regression fit lines in Figure 2. However, the bias always stays within the one standard deviation corridor. Therefore, the bias behavior as a function of buoy Qa ranges may be related in part to the collocation procedures (both, satellite data coverage and Qa depend on latitude), to differences in estimates of daily average buoy and satellite Qa, and to the impact of difference in the buoy and satellite temporal and spatial sampling schemes. Similar bias dependencies on Qa are present in comparisons with NOCS2.0 Qa (Figures 2c and 2d). Biases at buoy locations (where at least one year of collocated data are available) display weak geographical variations. Air humidity bias varies from -0.10g/kg to 0.10g/kg at the midlatitude MFUK locations, but the bias range increases in more humid tropical conditions where it varies from -0.30g/kg to 0.30g/kg at the tropical mooring locations, except at the 125°W, 2°S TAO mooring where the bias is anomalously strong reaching 0.90g/kg.

Standard deviation (STD) of daily satellite and in-situ (buoy and ship) specific air humidity is also weaker at midlatitudes and increases in the tropics (Table 1) changing from 0.79g/kg to 1.05g/kg. It depicts weak changes among buoy locations with the exception of higher values in the Mediterranean Sea where STD is about 1.10g/kg. At the two Mediterranean MFUK locations atmospheric conditions are strongly variable. For instance, STD of specific air humidity measured by MFUK buoy moored in the Mediterranean Sea is twice as strong as that at the Atlantic MFUK moorings. Better satellite data sampling is needed to STD between satellite and buoy data in the Mediterranean Sea.

The newly developed algorithm used to estimate satellite daily specific air humidity provides significant improvements compared to the previous one (Bentamy *et al*, 2003). Indeed, statistics characterizing comparisons between buoy and satellite, as well as NOCS2.0 and satellite clearly state that results are better for the updated Qasat in various study regions (Table 1). For instance, RMS difference values (estimated from bias and standard deviation values) are reduced by factor exceeding 50% between new and old daily satellite Qa estimates.

At global scale, the updated Qasat are compared with daily averaged 10m Qa from NOCS2.0 (Qanocs). The two Qa sources are collocated in space and time. For each day, Qasat values are linearly interpolated over Qamod grid map. The resulting collocated daily data are used to estimate monthly, seasonal, and annual statistical parameters, such as mean and standard deviation of each Qa product, mean and RMS differences , and correlation coefficient between Qanocs and Qasat (in this order). Only results derived from collocated data occurring during 2007 are shown. They are not used for calibration procedure dealing with the determination of the retrieval model (eq. 1).

Spatial variability of specific air humidity from the two products exhibit very similar features

for monthly as well as for seasonal and annual scales. The former are highly related to sea surface temperature and precipitation spatial patterns and meet the main known specific air humidity spatial distribution characteristics (Jackson *et al*, 2009). For instance, Figure 3 illustrates Qasat spatial patterns estimated for winter (December-January-February (DJF)), spring (March-April-May (MAM)), summer (June-July-August (JJA)), and autumn (September-October-November (SON)) north hemisphere seasons (NH). Qa values exceeding 18 g/kg are mainly found along the convergence zones in the tropical Atlantic, Pacific and Indian Ocean. High values reaching or exceeding 19g/kg are depicted in the western Pacific zone (warm pool) throughout the year, in the tropical and north eastern Indian Ocean areas during spring and summer seasons, respectively, and in the Caribbean and Gulf of Mexico during summertime. The seasonal variations result in significant differences between NH winter and summer specific air humidity estimates. They reach 6g/kg off north eastern oceanic regions, north of the Indian Ocean, Gulf of Mexico, over the entire Mediterranean sea, off the northwestern African coasts, and southeastern Indian Ocean. Such spatial and seasonal patterns are likely closely related to those of SST.

Insert Figure3

The spatial patterns of differences between NOCS2.0 and satellite Qa during NH winter and summer seasons are shown in Figure 4. Panels on top and on bottom illustrate bias and standard deviation differences, respectively. The new Qasat daily estimates reduce the discrepancies between in-situ and satellite in term of mean difference as well as in term of variability. Indeed, previous studies reported that IFREMER (old version) specific air humidity is 1g/kg underestimated compared to ICOADS over the intertropical ocean (Jackson *et al*, 2009), whereas is slightly overestimated over subtropical oceanic areas. Both statistical parameter spatial distributions (Figure 4) do not exhibit significant geophysical pattern dependency. More than 84% and 95% of Qa difference values are lower than 1g/kg and 1.5g/kg, respectively. Whereas the associated standard deviation values are lower than 2g/kg for 95% of total grid points. Most of the differences exceeding 1g/kg are found in the southern ocean and/or in regions where NOCS2.0 Qa error exceed 1.3g/kg associated with issues related to sampling by ships (Berry *et al*, 2011). Excluding these poorly sampled regions leads to an improvement of NOCS2.0 and satellite comparisons. More than 95% of differences do not exceed 1.20g/kg. At regional scales, two areas located in northwestern Atlantic and Pacific oceans and likely related to Gulf Stream and Kuroshio currents are depicted during NH winter season. Specific air humidity is assumed to be low (Figure 4) due to continental cold air outbreaks. These discrepancies might be partly related to the uncertainties of the retrieval model (eq. 1) at some specific locations and for some local atmospheric and oceanic conditions.

Insert Figure4

4. Daily Wind Fields

Surface wind speeds and directions may be retrieved from scatterometer and radiometers. In this study only QuikSCAT *V3* retrievals are used. As mentioned in section 2, they are corrected with respect to (Bentamy *et al*, 2012) results. The calculation of daily gridded wind fields from scatterometer wind observations is performed using same objective method used for the estimation of daily ASCAT wind fields (Bentamy *et al*, 2011). The resulting wind field accuracy is investigated trough the comparisons with daily-averaged winds from MFUK, NDBC, PIRATA, RAMA, and TAO moored buoy estimates. The main statistics characterizing scatterometer and buoy daily wind speeds and direction comparisons are summarized in Table 2. The overall statistics indicate that the daily scatterometer wind fields compare well to daily-averaged buoy data. The rms differences do not exceed 2m/s and 20°, which are the scatterometer specifications for wind speed and direction, respectively. For in-situ and scatterometer daily winds higher than 3m/s no significant bias trend is found. For lower wind speed ranges, scatterometer winds tend to be slightly overestimated compared to buoys. The wind direction biases are relatively small. Despite of difference in buoy and scatterometer sampling schemes used for the estimation of daily winds, correlation values attest that satellite daily winds reproduce fairly well in-situ estimates. The lowest correlation value is found for Tropical buoy and satellite wind comparisons due to the low wind speed conditions distribution in these specific oceanic regions.

5. Turbulent Fluxes

Daily surface wind stress and the associated zonal and meridional wind stress components, surface latent and sensible heat fluxes are estimated over global ocean from daily winds (section 4), specific air humidity (section 3), sea surface temperature and air temperature, utilizing COARE3.0 bulk parameterization (Fairall *et al*, 2003). SST are daily OI analyses (Reynolds et al, 2007), while Ta_{10} are daily averaged estimates calculated from Era Interim analyses (section 2). The calculations of the gridded bulk variables and turbulent flux fields are performed over global ocean with a spatial resolution of 0.25° in longitude and latitude. One should notice that flux fields spatial and temporal resolutions are consistent with SST analyses.

The quality of the new flux fields is first examined through comparisons with turbulent fluxes estimated from moored buoy daily-averaged bulk variables. Most of the NDBC buoys do not

provide measurements of specific air humidity (or relative humidity). They are calculated from air and dew point measurements. Daily turbulent fluxes are estimated utilizing COARE 3.0 parameterization. Therefore, any departures between buoy and satellite daily fluxes highlight differences in the daily bulk variables. In this paper statistics related to the comparisons between buoy and satellite daily wind stress (τ), latent (LHF) and sensible (SHF) heat fluxes are provided (Table 2). They are calculated from collocated buoy and satellite data during the 2005 – 2007 period.

As expected, buoy and satellite daily wind stress exhibit quite similar comparison results that found for wind speed (Table 2). This is clearly attested by the correlation coefficient values. Furthermore, the negative bias values are associated with the small overestimation of satellite wind speeds.

Daily satellite LHF is slightly underestimated in comparison with buoy data. The biases from the MFUK, NDBC, and tropical moorings are 5W/m², 13W/m², and 2W/m², respectively, correspondingly 7%, 12%, and 1% of the mean buoy LHF. Again we find rather high temporal correlation of satellite and in-situ turbulent fluxes (Table 2), which tend to decrease in the tropics. Remaining sampling issues result in moderately strong RMS errors (~30W/m² for MFUK and tropical moorings and somewhat stronger 37W/m² in the Atlantic western boundary sampled by NDBC moorings). The positive (buoy-minus-satellite) LHF biases at MFUK and NDBC locations are mainly related to the underestimation of high LHF>200W/m² at low Qa and/or for high winds. In fact, the satellite Qa is higher than in-situ Qa in dry conditions (Figure 2) that leads to LHF underestimation. Excluding cases with buoy Qa<3g/kg reduces satellite LHF biases down to 4W/m² (MFUK) and 6W/m² (NDBC) while the RMS error reduces to 25W/m² (MFUK) and 29W/m²(NDBC).

Satellite daily SHF has high correlation with in–situ data at extratropical locations and somewhat reduced correlation in the tropics (Table 2). The biases at MFUK and NDBC moorings are lower than 2W/m² in magnitude, which are negligible. In the tropics where time mean SHF is weak, satellite SHF is overestimated by 4 W/m^2. This departure is related to the underestimation of air temperature in warm and humid conditions (not shown). These comparisons show improvements of the new satellite SHF. Indeed, the previous version of SHF (Bentamy *et al*, 2007) was biased by more than 10W/m² according to Stantorelli *et al* (2011) .

For global comparisons we select NOCS2.0 daily LHF and SHF with uncertainties lower than 40W/m² and 20W/m², respectively. The above thresholds are the median values of NOCS2.0 LHF and SHF errors. They are chosen in order to keep enough in situ data for comparisons. Consequently, most of selected NOCS2.0 data are located in northern basins. The lowest NOCS2.0

data sampling is in the tropics and in the southern latitudes. In particular, there is a factor 20 between sampling lengths at 40°N and 40°S. The spatial distribution of the seasonal mean NOCS2.0 minus satellite LHF does not show any systematic basin scale patterns. The highest positive differences (NOCS2.0 – satellite> 30W/m²) are found in the Mediterranean Sea year around, and in the western boundaries during local winter. To summarize NOCS2.0 and satellite LHF comparisons, Figures 5 and 6 show zonally average fluxes stratified by basins. The two LHF data have similar latitudinal dependencies, especially in the north where in-situ data coverage is better. For both datasets the zonal mean LHF exceeds 100W/m² in the trade wind zones (Figures 5 and 6) where rather strong winds and dry air are both present. The seasonal variability, which is pronounced in the Atlantic and Pacific, is associated with stronger winds in local winter. Both, NOCS2.0 and satellite LHF indicate maxima along 40°N and 36°N in the Atlantic and Pacific, respectively during winter season (Figure 5) reflecting contributions from high LHF in the western boundaries associated with winter storms. These high LHF are absent in local summer (Figure 6). Locally weak LHF is present year around along the equator in the Atlantic and Pacific due to lower winds and rather cold SST in the eastern cold tong regions. The lowest LHF is found at high latitudes due to cold SST and related low air humidity. Due to the sampling issues, the discrepancies between NOCS2.0 and satellite LHF are stronger in southern oceans. For instance near 40°S in the Atlantic and Indian Oceans they exceed 30W/m² in boreal summer (Figure 6). Lower ship-based LHF may be linked to the need to avoid stormy sea. Indeed, 90% of NOCS2.0 daily LHF along 40°S in the Indian Ocean are lower than 50W/m², but this percentage is only of 20% for satellite daily LHF.

Insert Figures 5 and 6

Zonally average sensible heat fluxes from NOCS2.0 and satellite exhibit qualitatively similar behavior (Figures 7 and 8). Both SHF estimates do not exceed 20W/m² in the tropics and increases towards the midlatitudes of the winter hemisphere. The highest sensible heat loss occurs around 40°N in the Atlantic and Pacific in boreal winter due to high winds and strong air-sea temperature difference (ΔT) in the western boundary regions. The northern SHF amplification is not present in local summer reflecting significant seasonal drop in the storm track activity. Though the two SHF are highly correlated, satellite SHF is higher than NOCS2.0. The difference is apparent during local winter. It increases up to 25W/m² in the north Pacific between 30N and 40°N (Figure 7). Even higher differences occur in the South Ocean in austral winter (Figure 8). Discrepancies between NOCS2.0 and satellite SHF are more pronounced during summer season in regions located south of 40°S, where satellite SHF exhibits much more seasonal variation than NOCS2.0. Summertime

departures found at high southern latitudes are mainly associated with differences in wind speeds and to the poor temporal and spatial samplings of NOCS2.0 daily data and missing strong wind events, which are avoided by ships.

Insert Figures 7 and 8

6. Conclusion

The presence of notorious biases in the previous version of the IFREMER turbulent fluxes of Bentamy *et al*. (2003) requires improvement of the product. The availability of the new air-sea interaction gridded dataset (NOCS2.0) calculated from ICOADS data, allows an opportunity for satellite-derived turbulent flux enhancement over global ocean. The new version of the IFREMER satellite turbulent air-sea fluxes is based on improved air humidity (Qa) retrieval scheme, improved scatterometer wind retrievals, and adopting air temperature from Era Interim air temperature.

The core of the air humidity retrieval scheme remains unchanged. It is based on the statistical relationship between the microwave brightness temperatures and Qa, which in turn is based on the quasi-linear relationship between Qa and water vapor content (Schultz *et al*, 1993). But, direct application of this retrieval algorithm in Bentamy *et al*. (2003) results in SST-dependent Qa bias. This suggests including of SST as a parameter of satellite Qa retrieval model. Furthermore, the analysis of Qa bias reveals a dependence on the atmospheric stratification that reflects modifications in the relationship between water vapor content and Qa over the ocean SST fronts. Therefore, the new Qa retrieval algorithm includes SST and the air-sea temperature difference terms along with traditional microwave brightness terms. The retrieval model parameters are fitted using global in-situ data from the bias corrected version of ICOADS (NOCS2.0). The new satellite Qa has a reduced bias with in situ data that nor longer depicts the large scale patterns (dry tropics and wet subtropics) found in the previous IFREMER product.

The objective method developed and used for the estimation of daily surface wind analyses from scatterometer retrievals is adopted for the calculation of gridded daily Qa over global ocean with a spatial resolution of 0.25° in latitude and longitude. The validation of daily Qa estimates shows good statistic comparisons with daily Qa from moorings in the North Atlantic Ocean and in the tropical zones. The RMS values are about 1g/kg while correlation coefficients exceed 0.85. Similar results are obtained from the comparisons versus daily NOCS2.0 not used in the development of the satellite Qa model.

Using of the improved Qa retrieval, surface wind speed from the newly reprocessed

QuikSCAT data (QuikSCAT V3), 10m air temperature estimated from Era Interim re-analyses, results in significant improvement of the global turbulent fluxes. Daily satellite LHF is slightly underestimated in comparison with in-situ buoy data. LHF bias at the midlatitudes locations (MFUK and NDBC moorings) is 5W/m² (or 7% of the mean buoy LHF) and 13W/m² (12%), respectively. It decreases to 2W/m² (1%) at the tropical moorings. SHF is slightly overestimated by 2W/m² (11%) at MFUK, by 2W/m² (7%) at NDBC, and by 4W/m² (51%) at the tropical moorings. At global scale, satellite-derived LHF and SHF exhibit similar spatial and temporal patterns that derived from NOCS2.0. Global comparisons between NOCS2.0 and satellite suggest that both, LHF and SHF exceed in-situ values in the storm track belts during local winter, which are particularly evident at high southern latitudes. The increased difference in the south is in part explained by the poor temporal and spatial samplings of NOCS2.0 daily data and missing strong wind events, which are avoided by ships. Indeed, 90% of NOCS2.0 daily LHF along 40°S in the Indian Ocean are lower than 50W/m², but this percentage is only of 20% for satellite daily LHF.

The statistical comparisons between in-situ (moorings and NOCS2.0) and satellite bulk variables and turbulent fluxes assess the improvement of the new calculations with regards to the previous IFREMER satellite flux accuracy. In future, flux calculation will be first performed for the whole QuikSCAT period (August 1999 – November 2009). The spatial and temporal patterns of the resulting flux fields will be investigated and compared to those derived from satellite observations such as HOAPS, from blended data such as AOFLUX, or from meteorological re-analyses such as Era Interim. The extension of the calculation to the periods of the European Satellite Remote Sensing satellites ERS-1 and ERS-2 (March 1992 – January 2001), and of ASCAT (February 2007 – Present) is expected.

Acknowledgements. This research was supported by TOSCA (Terre, Océan, Surfaces continentales, Atmosphère) and SIMED ((Simulation de la MEDiterranée) projects, and by the NFS grant *ATM0631685*NASA. We thank D. Crozé-fillon, F. Paul, and J. F. Piollé and IFREMER/CERSAT for data processing support. The authors are grateful to ECMWF, EUMETSAT, CERSAT, JPL, NOAA, NOCS, Météo-France, NDBC, PMEL, and UK MetOffice for providing numerical, satellite, and in-situ data used in this study.

References

Andersson A., K. Fennig, C. Klepp, S. Bakan, H. Graßl, and J. Schulz, 2010: The Hamburg Ocean Atmosphere Parameters and Fluxes from Satellite Data - HOAPS-3, *Earth Syst. Sci. Data*, **2**, 215-234, doi:10.5194/essd-2-215-2010.

Ayina L. H., A. Bentamy, A. Mestas-Nunez, G. Madec, 2006: The impact of satellite winds and latent heat fluxes in a numerical simulation of the tropical Pacific Ocean. *Journal of Climate*, 19(22), 5889-5902. http://dx.doi.org/10.1175/JCLI3939.1

Bentamy A., K. Katsaros, A. Mestas-Nuñez, W. Drennan, E. Ford,H. Roquet , 2003: Satellite estimates of wind speed and latent heat flux over the global oceans. *Journal Of Climate*, 16(4), 637-656. http://dx.doi.org/10.1175/15200442(2003)016<0637:SEOWSA>2.0.CO;2

Bentamy A., L-H Ayina, W. Drennan, K. Katsaros, A. Mestas-nuñez, and R. T. Pinker, 2008: 15 years of ocean surface momentum and heat fluxes from remotely sensed observations. FLUXNEWS, No 5, World Climate Research Program, Geneva, Switzerland, 14-16

Bentamy A., D. Croizé. Fillon, 2011: Gridded Surface Wind Fields from Metop/ASCAT Measurements. Inter. Journal of Remote Sensing, 33, pp 1729-1754.

Bentamy, A., S. A. Grodsky, J. A. Carton, D. Croizé-Fillon, and B. Chapron, 2012: Matching ASCAT and QuikSCAT Winds, *J. Geoph. Res*., doi:10.1029/2011JC007479,

Berry, D.I. and E.C. Kent, 2011, Air-sea fluxes from NOCS2.0: the construction of a new gridded dataset with uncertainty estimates. *Int. J. Climatol.* (CLIMAR-III Special Issue), **31**, 987-1001 (doi:10.1002/joc.2059).

Bourras D., 2006: Comparison of Five Satellite-Derived Latent Heat Flux Products to Moored Buoy Data. *Journal of Climate*, Vol. 19, 2006, pp. 6291-6313. doi:10.1175/JCLI3977.1

Chou, S.-H., E. Nelkin, J. Ardizzone, R. M. Atlas, and C.-L. Shie, 2003: Surface turbulent heat and momentum fluxes over global oceans based on the Goddard satellite retrieval, version 2 (GSSTF2). *J. Climate*, **16**, 3256–3273.

Fairall, C.W., E.F Bradley, J.E. Hare, A.A. Grachev, and J.B. Edson (2003), Bulk parameterization of air-sea fluxes: updates and verification for the COARE3.0 algorithm, *J. Climate*, *16*, 571-591.

Fore A., B. Stiles, R. S. Dunbar, B. Williams, A. Chau, L. Ricciardulli, F. Wentz, T. Meissner and E. Rodridguez, 2011: Point-wise wind retrieval and ambiguity removal improvements for the QuikSCAT climatological data set. International Ocean Vector Wind Science Team Meeting Annapolis, Maryland, USA, 9-11 May 2011 (http://coaps.fsu.edu/scatterometry/meeting/past.php#2011)

Grodsky S. A., A. Bentamy, J. A. Carton, R. T. Pinker, 2009: Intraseasonal Latent Heat Flux Based on Satellite Observations. *Journal of Climate*, 22(17), 4539-4556. http://dx.doi.org/10.1175/2009JCLI2901.1

Jackson, D. L., G. A. Wick, and F. R. Robertson, 2009: Improved Multisensor Approach to Satellite-retrieved Near-surface Specific Humidity Observations. *J. Geophys. Res.*, D16303, doi:10.1029/2008JD011341.

JPL, 2006: QuikScat science data product user's manual (version 2.0). Jet Propulsion Laboratory Publ. D-18053, Pasadena, CA, 84pp. (Available online at http://podaac.jpl.nasa.gov/quikscat)

Kent E., S. D. Woodruff, and D. I. Berry, 2007: Metadata from WMO Publication No. 47 and an assessment of Voluntary Observing Ship observation heights in NOCS2.0. *J. Atmos. Oceanic Technol.*, 24**,** 214–234.

Kubota, M., N. Iwasaka, S. Kizu, M. Konda & K. Kutsuwada , 2002: Japanese ocean flux data sets with use of remote sensing observations (J-OFURO), *J. Oceanogr.*, 58, 213-225.

Ricciardulli L. and F. Wentz, 2011: Reprocessed QuikSCAT (V04) wind vectors with Ku-2011 geophysical model function. Remote Sensing Systems Technical Report 043011 (http://www.ssmi.com/qscat/qscat_Ku2011_tech_report.pdf)

Meissner, T., D. K. Smith and F. J. Wentz, 2001: A 10-Year Intercomparison Between Collocated Special Sensor Microwave Imager Oceanic Surface Wind Speed Retrievals and Global Analyses, Journal of Geophysical Research, 106(C6), 11731-11742.

Mestas-Nuñez A., A. Bentamy, K. Kristina, 2006: Seasonal and El Nino variability in weekly satellite evaporation over the global ocean during 1996-98. *Journal Of Climate*, 19(10), 2025-2035. http://dx.doi.org/10.1175/JCLI3721.1

Reynolds, R.W., T.M. Smith, C. Liu, D.B. Chelton, K.S. Casey, M.G. Schlax (2007), Daily High-Resolution-Blended Analyses for Sea Surface Temperature. *J. Climate*, *20*, 5473-5496.

Santorelli, A., R. T. Pinker, A. Bentamy, W. Drennan, K. Katsaros, J. Carton, and A. Mestas-Nunez, 2011. *J. Geophys. Res*., 116, Article Number: C09028 DOI: 10.1029/2010JC006927

Schulz, J., P. Schlussel, and H. Grassl, 1993: Water vapour in the atmosphere boundary layer over oceans from SSM/I measurements. *Int. J. Remote. Sensing*, 14, 2773-2789.

Tomita,H. and M. Kubota, 2006: An analysis of the accuracy of Japanese Ocean Flux data sets with Use of Remote sensing Observations(J-OFURO) satellite-derived latent heat flux using moored buoy data,*J. Geophys. Res*, 111, C07007, doi:10,1029/2005 JC003013, 2006.

Wackernagel, H., 1998. Multivariate geostatistics. *Springer*, Berlin, 291pp.

Yu, L., R. A. Weller, and B. Sun, 2004: Improving latent and sensible heat flux estimates for the Atlantic Ocean (1988-1999) by a synthesis approach. *J. Climate*, 17, 373–393.

Tables

Table 1 : Statistical parameters of differences between daily buoy (MFUK, TAO, PIRATA,RAMA) and satellite specific air humidity estimated for the period 2005 –2007. Bias, STD, and Cor stand for mean and standard deviation difference (Buoy minus satellite) values, and correlation coefficients, respectively. Bias and Std are in g/kg units.

		Qasat			**Qasat_old**		
	Length	Bias	STD	Cor	Bias	Std	Cor
MFUK	2910	-0.04	0.87	0.95	-0.20	1.43	0.90
TAO/PIRATA/RAMA	16999	-0.10	1.05	0.85	0.88	1.62	0.75
NOCS2.0(MFUK)	67104	0.23	0.79	0.95	0.42	1.57	0.88
NOCS2.0(Tropical)	129341	0.27	1.05	0.83	0.74	1.55	0.73

Table 2: **:** Statistical parameters of differences between daily buoy (MFUK, NDBC, TAO, PIRATA,RAMA(Tropical)) and satellite wind speeds (Speed in m/s), wind directions (direction in degree), wind stress amplitude (Stress in dyn/m²), latent (LHF) and sensible (SHF) heat fluxes (in W/m²). Numbers to the right of mooring names are sampling length of buoy and satellite collocated daily data.

	MFUK(12146)			NDBC(28048)			Tropical(49843)		
	Bias	STD	Cor.	Bias	STD	Cor.	Bias	STD	Cor.
Speed	-0.36	1.58	0.92	-0.27	1.09	0.94	-0.25	1.25	0.85
Direction	0	19	1.76	-5	23	1.74	-4	17	1.65
Stress	-0.01	0.07	0.92	-0.01	0.04	0.95	-0.01	0.03	0.85
LHF	5	27	0.89	13	37	0.89	2	31	0.79
SHF	-2	10	0.94	-2	10	0.96	-4	6	0.77

Figure captions

- Figure 1 : NOCS2.0 minus satellite Qa_{10} difference as a function of satellite Qa_{10}. Lines are average difference in 1g/kg satellite Qa_{10} bin for data grouped in the five SST bins. Satellite (Ifremer) Qa_{10} is from Bentamy et al (2003).
- Figure 2 : Daily-averaged specific air humidity from buoys (MFUK(a) and Tropical(b)) and satellites. Panels c and d show companion comparisons with daily NOCS2.0 Qa from the two areas surrounding MFUK and tropical arrays, respectively. Black and red lines are perfect and symmetrical linear fit, respectively. Inner and outer dashed lines show one and two standard deviations of in-situ minus satellite Qa, respectively. Numbers in the color bars represent the number of collocated data per 0.50g/kg bins. Only bins such as the number of collocated data exceeding a threshold (30 for mooring and 100 for NOCS2.0 comparisons) are shown. The rest of collocated data are shown in gray dots.
- Figure 3: North hemisphere winter (DJF), spring (MAM), summer(JJA), and fall (SON) mean Qa_{10} patterns estimated from daily satellite analyses for the period: 2005 – 2007
- Figure 4: Seasonal patterns of mean (top) and standard deviation (bottom) differences between daily NOCS2.0 and satellite Qa_{10} estimated for 2005 – 2007 wintertime (DJF) and summertime(JJA).
- Figure 5: North hemisphere winter (DJF), spring (MAM), summer(JJA), and fall (SON) mean Qa_{10} patterns estimated from daily satellite analyses for the period: 2005 – 2007.
- Figure 6: As Figure 5 for summertime
- Figure 7: Latitudinal averages of NOCS2.0 (red color) and satellite (blue color) of SHF estimated over the Atlantic (left), the Pacific (middle), and the Indian (right) oceans for 2005-2007 wintertime.
- Figure 8: As Figure 7 for summertime

Figures

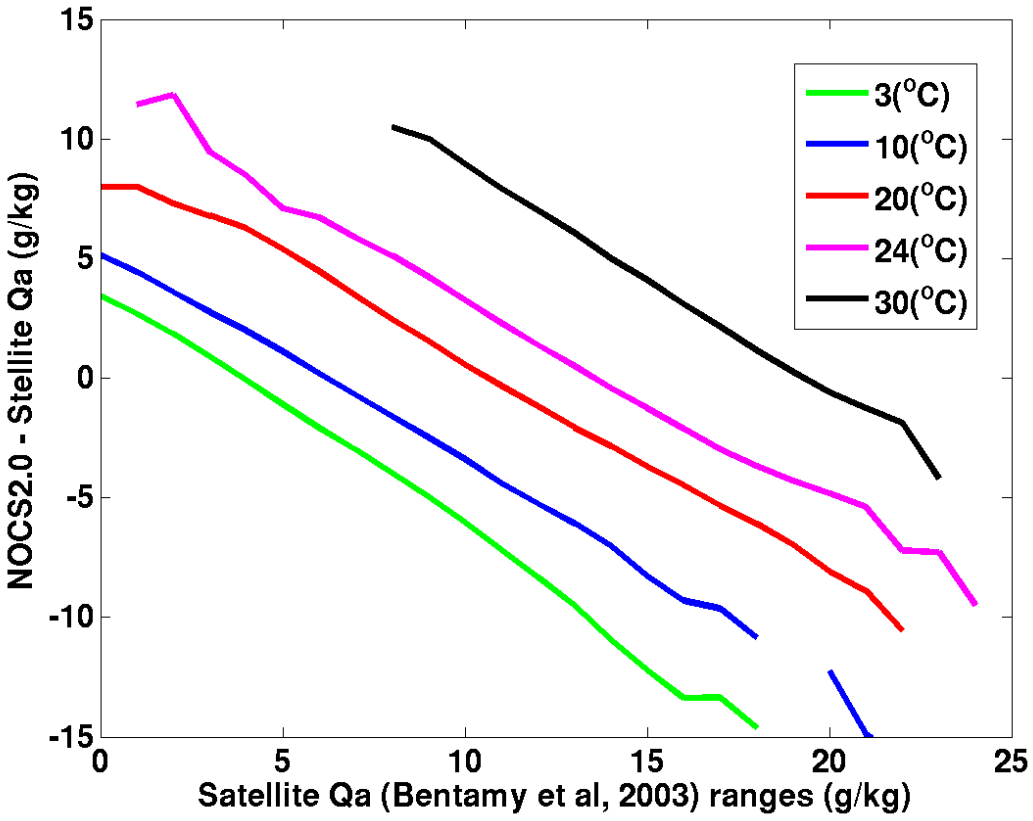

Figure 1 : NOCS2.0 minus satellite Qa_{10} difference as a function of satellite Qa_{10}. Lines are average difference in 1g/kg satellite Qa_{10} bin for data grouped in the five SST bins. Satellite (Ifremer) Qa_{10} is from Bentamy et al (2003).

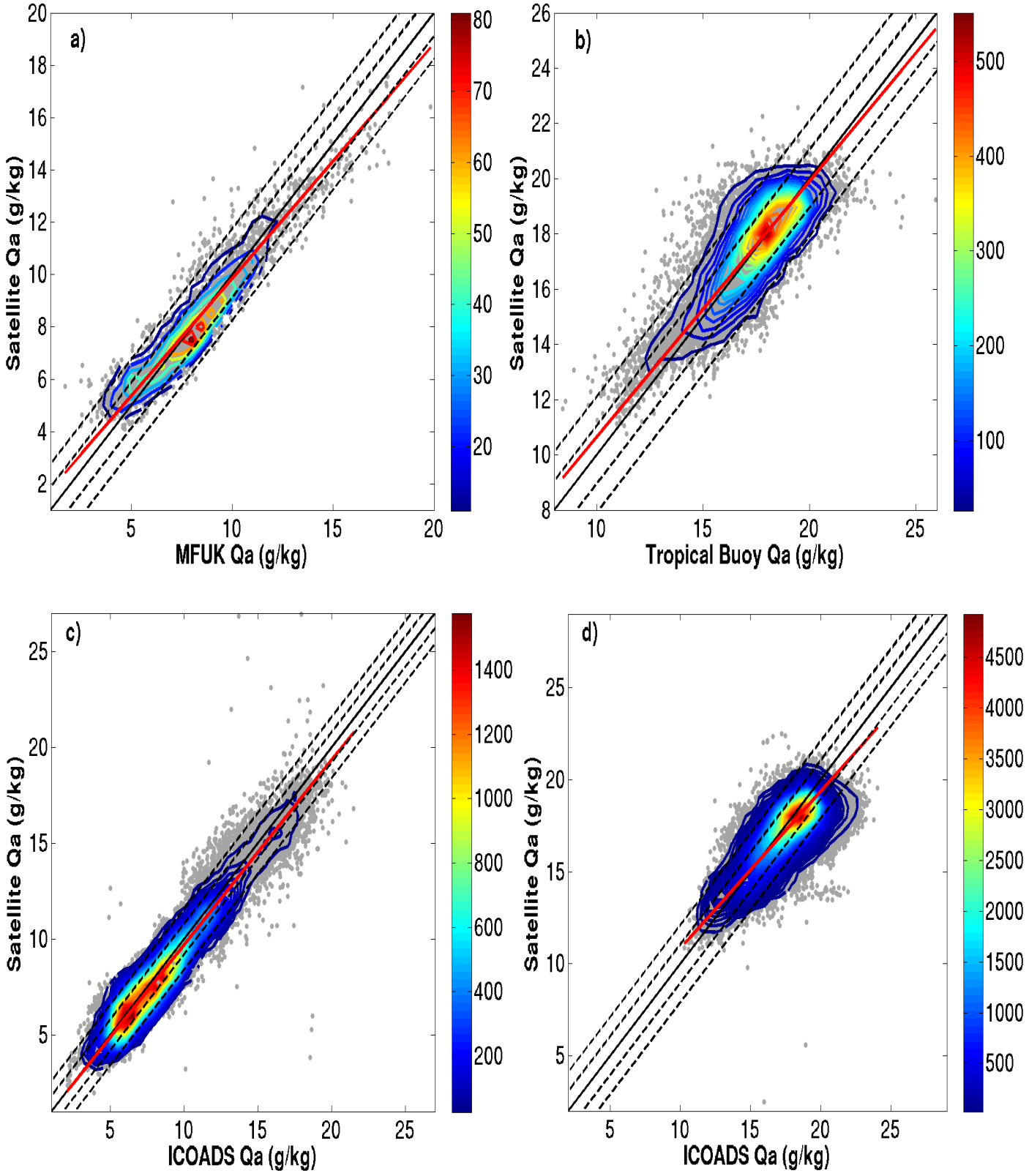

Figure 2 : Daily-averaged specific air humidity from buoys (MFUK(a) and Tropical(b)) and satellites. Panels c and d show companion comparisons with daily NOCS2.0 Qa from the two areas surrounding MFUK and tropical arrays, respectively. Black and red lines are perfect and symmetrical linear fit, respectively. Inner and outer dashed lines show one and two standard deviations of in-situ minus satellite Qa, respectively. Numbers in the color bars represent the number of collocated data per 0.50g/kg bins. Only bins such as the number of collocated data exceeding a threshold (30 for mooring and 100 for NOCS2.0 comparisons) are shown. The rest of collocated data are shown in gray dots.

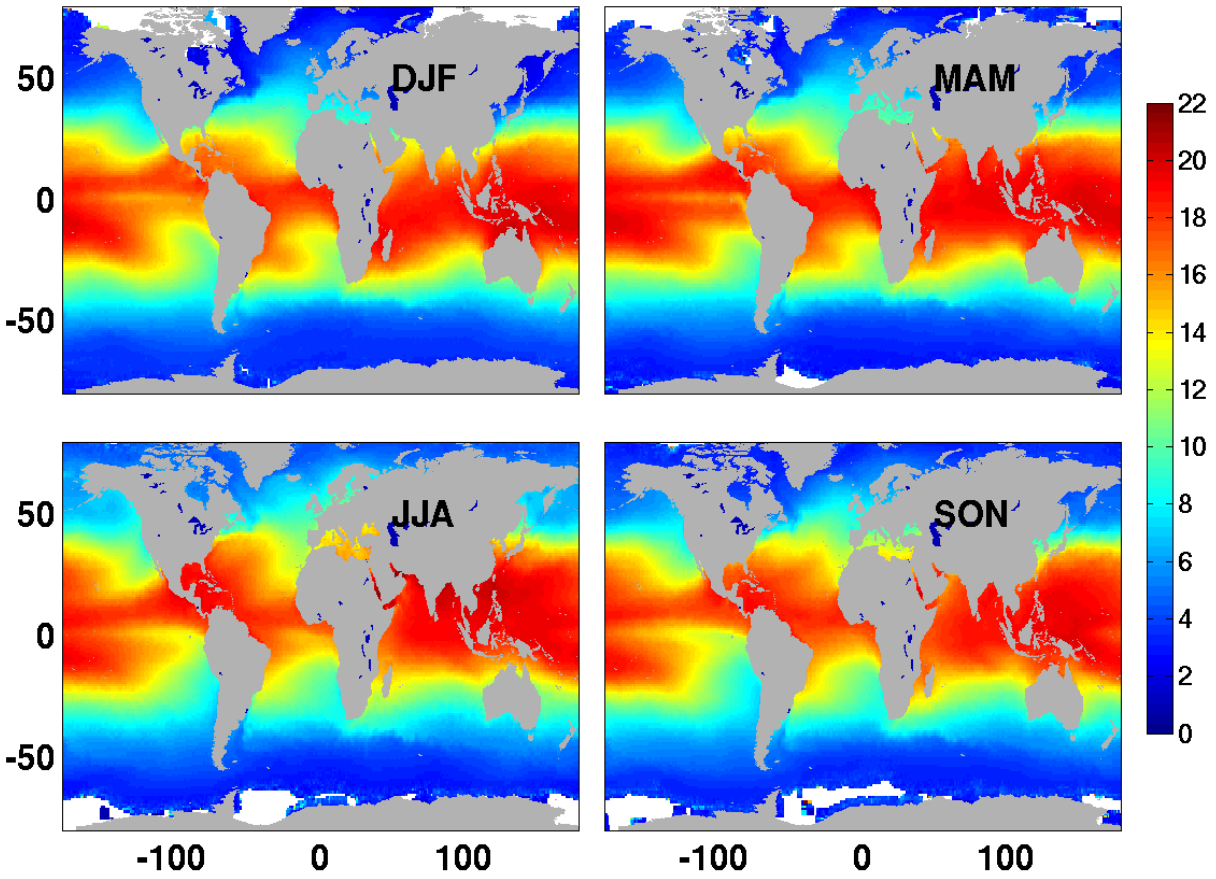

Figure 3 : North hemisphere winter (DJF), spring (MAM), summer(JJA), and fall (SON) mean Qa_{10} patterns estimated from daily satellite analyses for the period: 2005 – 2007.

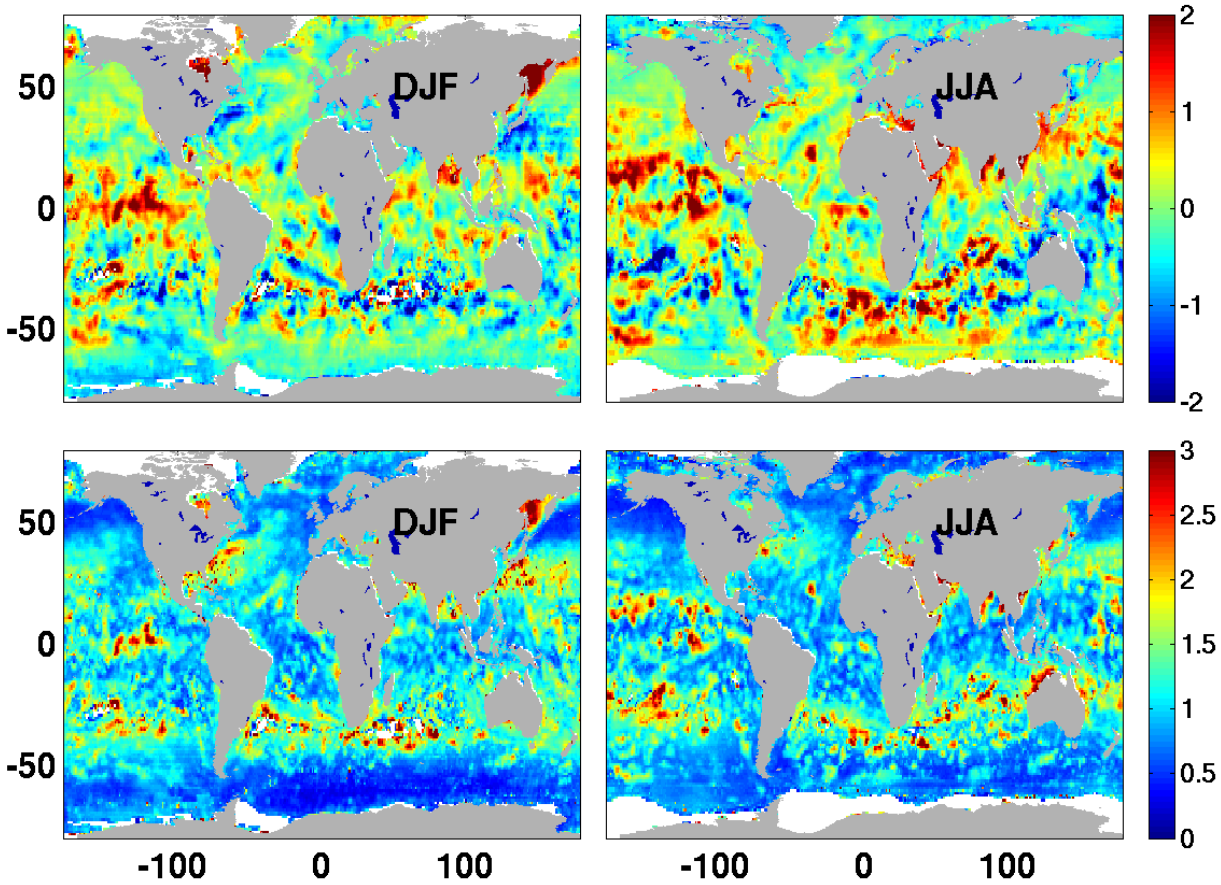

Figure 4 : Seasonal patterns of mean (top) and standard deviation (bottom) differences between daily NOCS2.0 and satellite Qa_{10} estimated for 2005 – 2007 wintertime (DJF) and summertime(JJA).

1

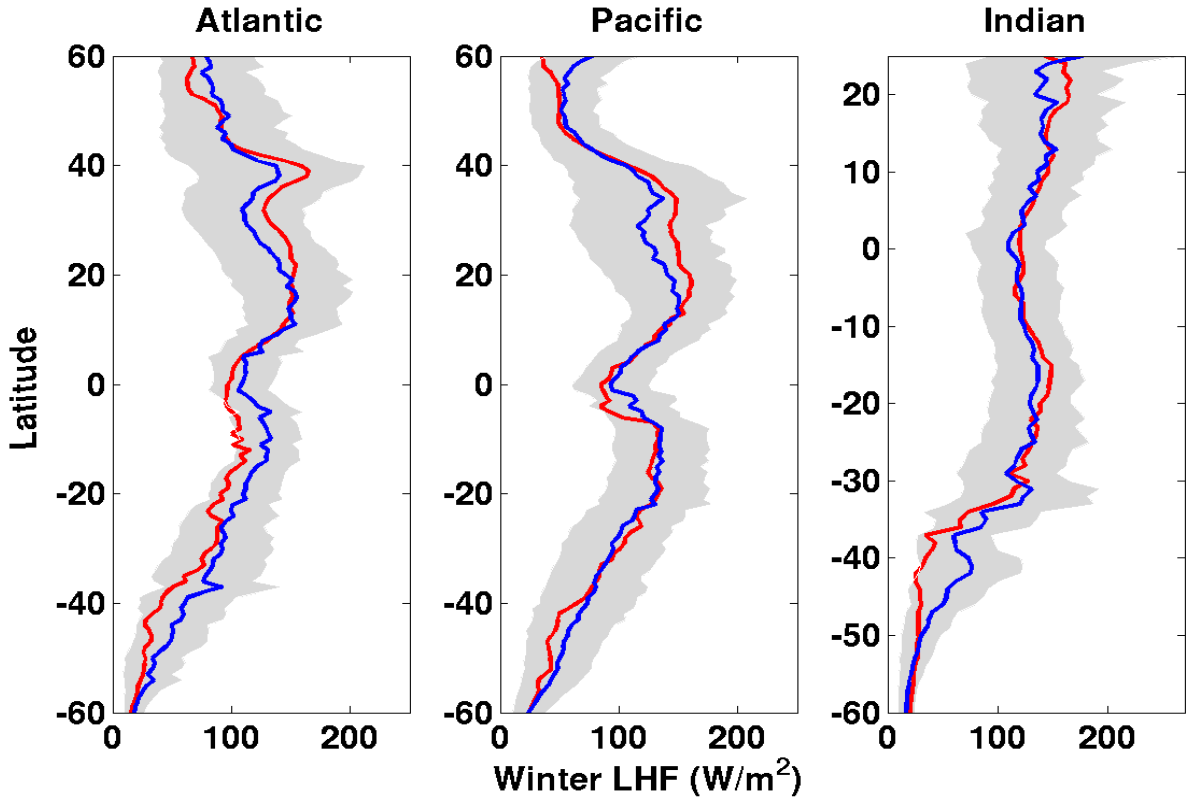

Figure 5 : Latitudinal averages of NOCS2.0 (red color) and satellite (blue color) of LHF estimated over the Atlantic (left), the Pacific (middle), and the Indian (right) oceans for 2005-2007 wintertime.

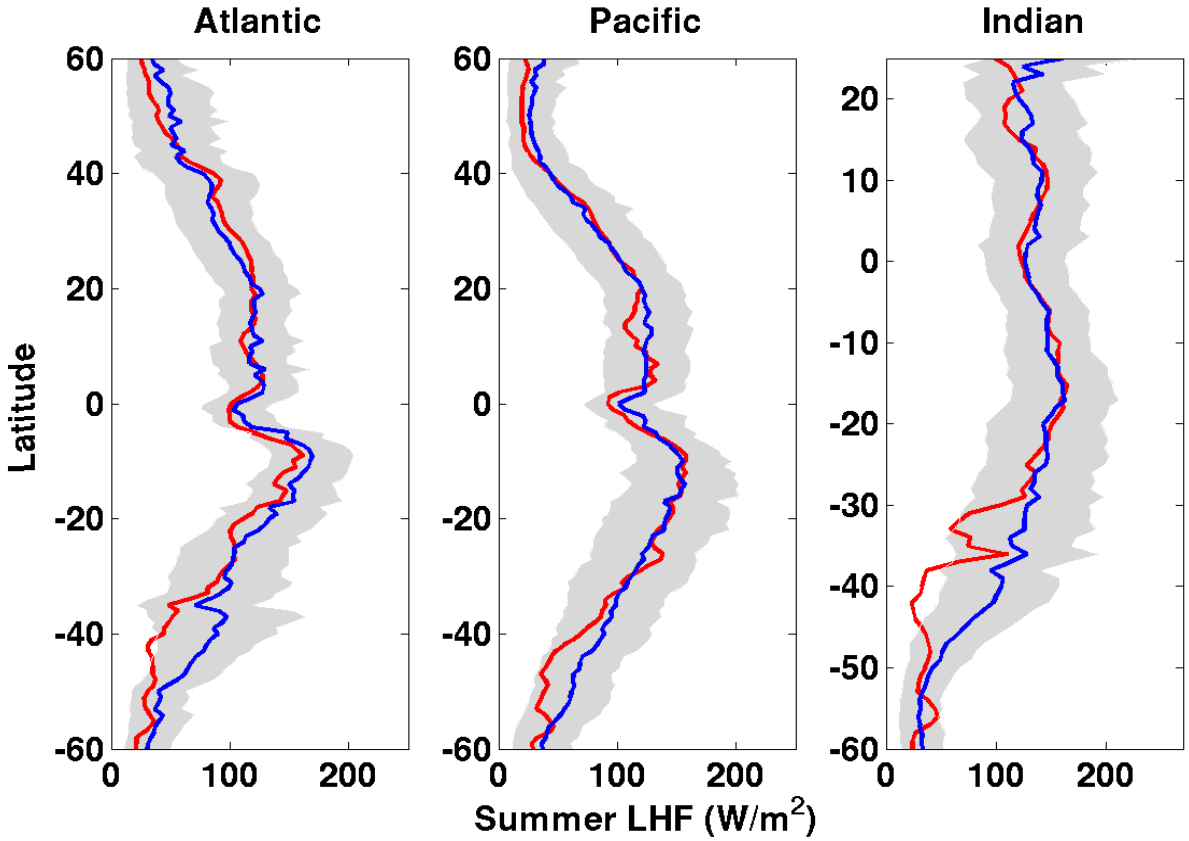

Figure 6 : As Figure 5 for summertime

1

2

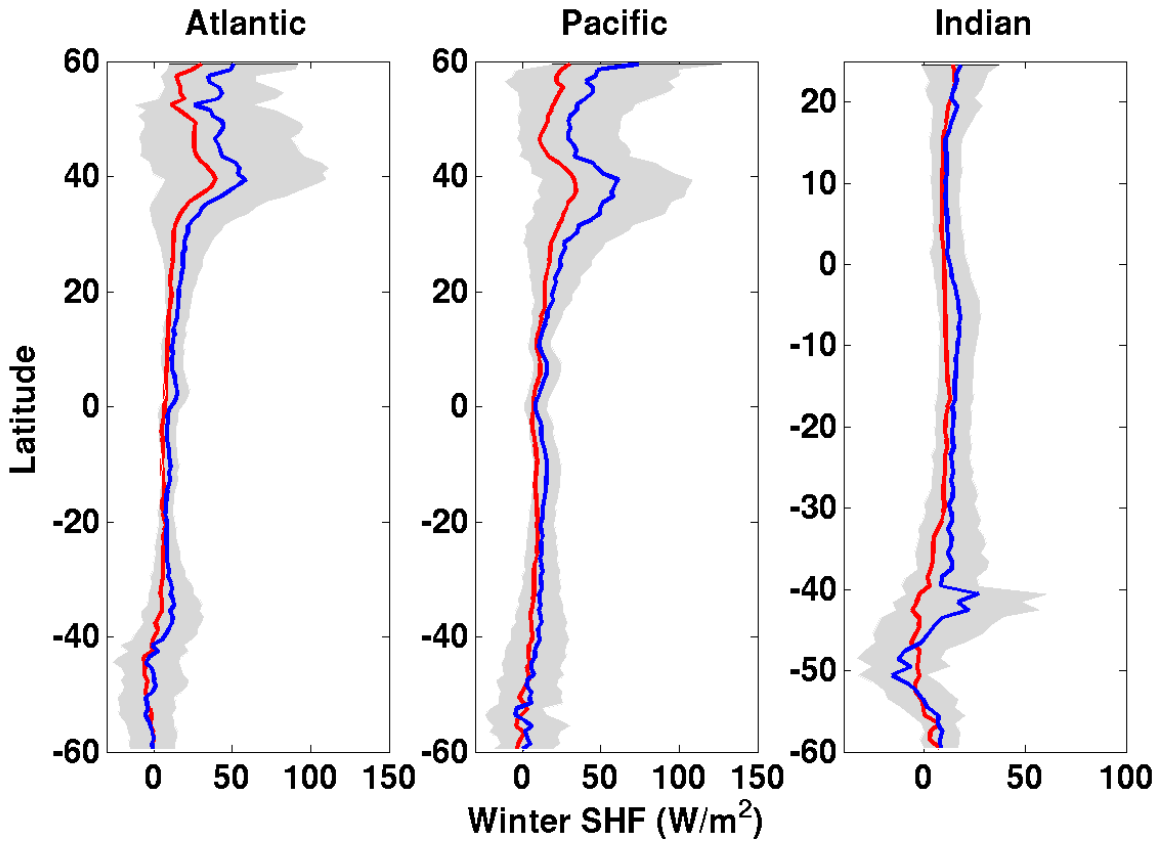

Figure 7 : : Latitudinal averages of NOCS2.0 (red color) and satellite (blue color) of SHF estimated over the Atlantic (left), the Pacific (middle), and the Indian (right) oceans for 2005-2007 wintertime.

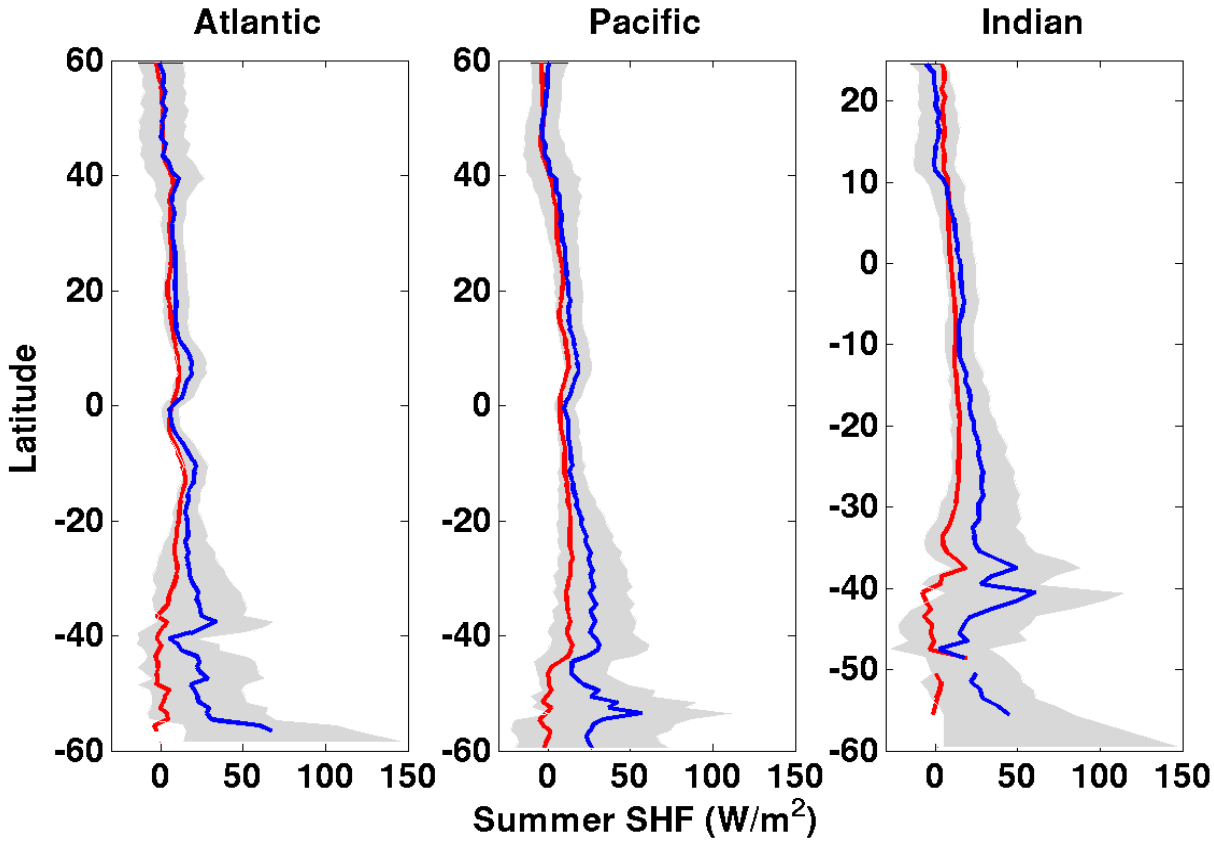

Figure 8 : As Figure 7 for summertime.